Sensors and Materials, Vol. 10, No. 7 (1998) 405–412
MYU Tokyo

S & M 0342

Application of Harmonic Finite Element Analysis to a CMOS Heat-Capacity Measurement Structure

Markus Emmenegger, Jan G. Korvink[1], Martin Bächtold,
Martin von Arx, Oliver Paul and Henry Baltes

Physical Electronics Laboratory, ETH Zurich, CH-8093 Zurich, Switzerland
[1]Albert Ludwig University, D-79110 Freiburg, Germany

(Received March 18, 1997; accepted December 1, 1997)

***Key words*:** microsystem modeling, harmonic analysis, material characterization, finite elements, heat capacity

We present the application of time-harmonic finite element techniques to model the behavior of CMOS test structures. Our test structures are designed to measure the heat capacity of CMOS thin films. The dynamic nature of heat capacity implies a time-dependent approach for both measurement and simulation. The devices are excited by AC heating. A 3-D finite element analysis tool incorporating harmonic time-dependent analysis capabilities has been developed to simulate the behavior of such devices. We verify our method by comparing the results of simulations and measurements with the device.

1. Introduction

The characterization of thermal properties of materials is crucial for the design and optimization of microsensors. The materials available in standard IC processes are thin films to which bulk material parameters do not necessarily apply. Special test structures are required to characterize these films. A test structure has been developed(1) to measure the specific heat of thin films. The specific heat determines the dynamic behavior of thermal microsystems; it is therefore important in all time-critical applications. Its dynamic nature implies a time-dependent approach for the measurement. In the setup presented here, AC heating is applied, and the frequency-dependent response of the system is measured.

An analytical model(1) of the AC response of the structure was developed to extract the material properties from the measurement. The validity of this model rests on a number of assumptions concerning the form of the temperature field. To verify these assumptions, numerical simulations were performed. We have incorporated thermal AC analysis into our finite element framework and calculated the temperature distribution on the device to verify if a lumped, one-dimensional model is applicable.

2. Test Structure

The test structure is shown in Figs. 1(a) and 1(b). A 200-μm-long freestanding cantilever is formed using the dielectric layers. It contains both the gate polysilicon and the metallization layer. At the front of the cantilever, a heating resistor made of polysilicon is integrated. The resistor contacts four metal lines for accurate determination of dissipated power. Eight polysilicon stripes are integrated into the cantilever, running from the heating resistor to the silicon support. The contact of these stripes to metal structures at different positions allows the temperature to be measured at different points on the cantilever by means of the Seebeck effect. The Seebeck coefficient, which relates the temperatures to

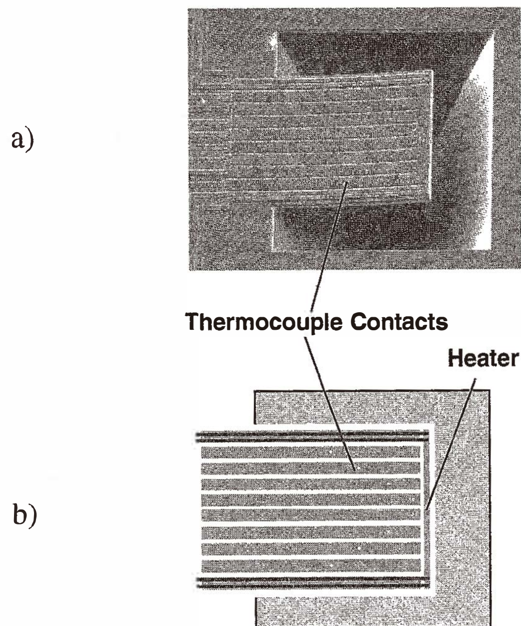

Fig. 1. (a) Micrograph and (b) schematic mask layout of the CMOS heat capacity characterization structure. The underetched cavity ensures thermal insulation of the protruding beam sandwich.

the measured voltages, has been determined separately.[2] The device is operated under vacuum, forcing the heat to flow only along the cantilever into the substrate. When the heater is fed with a sinusoidal current, temperature oscillation occurs in the heater. This oscillation propagates along the cantilever. Because the thermal time constants are short in such a small system, it is possible to obtain sinusoidally varying temperatures with frequencies in the range of 100 Hz. The amplitudes and phases of the oscillations are measured at the four thermocouple contacts. The temperature distribution depends on the frequency, the thermal conductivity, and the heat capacity of the materials. The thermal conductivity is extracted from a static measurement, and the heat capacity is evaluated from AC results.

3. Analytical Model

The governing equation for thermal effects is the heat transfer equation, which is given by[3]

$$c(\boldsymbol{x})\frac{\partial}{\partial t}T(\boldsymbol{x},t)-\nabla\cdot\left(\kappa(\boldsymbol{x})\nabla T(\boldsymbol{x},t)\right)=P(\boldsymbol{x},t), \tag{1}$$

where $T(\boldsymbol{x},t)$, $P(\boldsymbol{x},t)$, $c(\boldsymbol{x})$, $\kappa(\boldsymbol{x})$ and t denote the temperature distribution in time and space, the density of the heat power source, the volumetric heat capacity, the heat conductivity tensor and the time, respectively. Furthermore, conditions must be specified on the boundary of the solution domain. We apply frequency domain analysis to this problem. Assuming that all heat sources and boundary conditions vary sinusoidally in time, the temperature varies sinusoidally as well (i denotes $\sqrt{-1}$):

$$P(\boldsymbol{x},t)=P(\boldsymbol{x})e^{\mathrm{i}\omega t} \tag{2}$$

$$T(\boldsymbol{x},t)=T(\boldsymbol{x})e^{\mathrm{i}\omega t} \tag{3}$$

From eq. (1), a complexly valued partial differential equation is obtained:

$$c(\boldsymbol{x})\mathrm{i}\omega T(\boldsymbol{x},\omega)-\nabla\cdot\left(\kappa(\boldsymbol{x})\nabla T(\boldsymbol{x},\omega)\right)=P(\boldsymbol{x},\omega). \tag{4}$$

The complex temperature distribution is time-independent, and the complex value at each point in space gives the phase and amplitude of the temperature oscillation. If no heat sources exist inside the solution domain and the heat capacitance and thermal conductivities are constant in the domain, the equation has the following analytical solution for a one-dimensional geometry:

$$T(x,\omega) = Ae^{\beta x}e^{i\beta x} + Be^{-\beta x}e^{-i\beta x}, \tag{5}$$

where A and B are complex integration constants determined by the boundary conditions, and β is given by

$$\beta = \sqrt{\frac{\omega}{2} \cdot \frac{c}{\kappa}}. \tag{6}$$

The solution has the form of an exponentially damped thermal wave. The damping length is proportional to the square root of the thermal diffusivity, i.e., the ratio of the specific heat and the thermal conductivity. Note that this simple model is restricted to a device where the temperature and phase distribution vary in one dimension only. The test structures were designed in view of the application of such a one-dimensional model. To check if this assumption is valid for the test structure, a full, 3-D numerical analysis was performed.

4. 3-D Numerical Simulation

To solve the heat transfer equation numerically, a spatial discretization is necessary. We use the finite element method, but the approach presented here is valid for other discretization schemes. A discretization method transforms the partial differential equation into a set of ordinary differential equations; in the case of linear heat conduction, the resulting equation is:[3]

$$\boldsymbol{K}\boldsymbol{u}(t) + \boldsymbol{M}\frac{d}{dt}\boldsymbol{u}(t) = \boldsymbol{f}(t) \tag{7}$$

where $\boldsymbol{K}$ and $\boldsymbol{M}$ denote the real, symmetric, positive definite conductance and capacitance matrices, $\boldsymbol{u}$, the vector of the temperatures at the finite element nodes, $\boldsymbol{f}$, the heat source and boundary condition terms, and t, the time. To solve this system of ordinary differential equations, frequency domain or harmonic analysis may be used the same way as for the continuous case. Assuming harmonic time-dependence of all sources and temperatures, i.e.,

$$\boldsymbol{f}(t) = \boldsymbol{f}(\omega)e^{i\omega t} \tag{8}$$

$$\boldsymbol{u}(t) = \boldsymbol{u}(\omega)e^{i\omega t}, \tag{9}$$

a complex, linear algebraic equation system

$$\boldsymbol{K}\boldsymbol{u}(\omega) + i\omega\boldsymbol{M}\boldsymbol{u}(\omega) = \boldsymbol{f}(\omega) \tag{10}$$

is obtained, where the vector $\boldsymbol{u}$ now denotes complex quantities at the node points, specifying the amplitude and phase of the harmonically varying temperature. For each distinct frequency, a complex linear equation system must be solved. We now write the solution and the excitation in terms of their real and imaginary parts:

$$\begin{aligned} \boldsymbol{u}(\omega) &= \boldsymbol{u}_r(\omega) + \mathrm{i}\boldsymbol{u}_i(\omega) \\ \boldsymbol{f}(\omega) &= \boldsymbol{f}_r(\omega) + \mathrm{i}\boldsymbol{f}_i(\omega). \end{aligned} \tag{11}$$

We insert eq. (11) into eq. (10) and separately collect the real and imaginary parts,

$$\left(\boldsymbol{K}\boldsymbol{u}_r(\omega) + \omega\boldsymbol{M}\boldsymbol{u}_i(\omega)\right) + \mathrm{i}\left(\boldsymbol{K}\boldsymbol{u}_i(\omega) + \omega\boldsymbol{M}\boldsymbol{u}_r(\omega)\right) = \boldsymbol{f}_r(\omega) + \mathrm{i}\boldsymbol{f}_i(\omega) \tag{12}$$

yielding a real, nonsymmetric linear equation system of double size:

$$\begin{bmatrix} \boldsymbol{K} & -\omega\boldsymbol{M} \\ \omega\boldsymbol{M} & \boldsymbol{K} \end{bmatrix} \begin{bmatrix} \boldsymbol{u}_r \\ \boldsymbol{u}_i \end{bmatrix} = \begin{bmatrix} \boldsymbol{f}_r \\ \boldsymbol{f}_i \end{bmatrix} \tag{13}$$

This system is solved by a standard linear solver for real, nonsymmetric linear equations. Using this technique, frequency sweeps are simulated. In principle, it is possible to calculate the response of the system to any given signal using Fourier transformation. The harmonic method has been implemented into our finite element framework, and calculations have been made on a model of our heat capacity characterization device.

5. Results

Two different designs of the measurement structure were simulated. In the first structure, termed the reference device, the entire top is covered by the metallization. In the second structure, termed the stripe device, the metal area is reduced to 6-μm-wide stripes separated by 14 μm. The cross-sectional areas of metal and dielectrics are therefore different in these two devices. Comparison of the two structures allows the separation of the thermal properties of the dielectrics and the metallization.

The 3-D finite element model of the reference device was constructed and is shown in Fig. 2. The thermal conductivity and heat capacity were deduced from measurements using the one-dimensional analytical model described in ref. (1). These material parameters were used to perform a 3-D simulation. The temperature field was examined for uniformity across the cantilever. The amplitude and phase varied less than 0.3% and 0.2°, respectively, along any cut perpendicular to the heat flow. Therefore, the conditions for applying the one-dimensional model were satisfied. In the next step, the simulations were compared with the measurements. Figures 3(a) and 3(b) show the frequency-dependent temperature amplitudes and phases at the thermocouple contacts. The agreement between

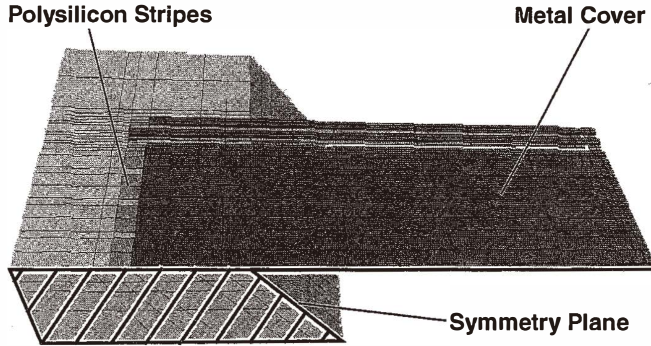

Fig. 2. Finite element model of the device shown in Fig. 1. The mesh corresponding to the dielectric layers has been removed to reveal the inner structure. The symmetry plane represents a homogenous Neumann boundary condition. The extremities of the silicon wafer are kept at ambient temperature by a Dirichlet boundary condition. Because the device is operated in vacuum, the cavity is not included in the simulation.

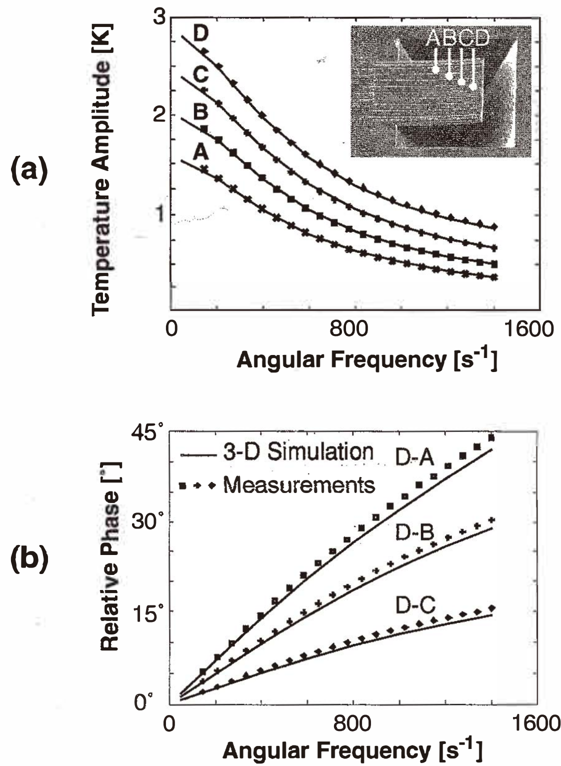

Fig. 3. Simulation results (solid lines) and measurements (dots) at each thermocouple contact. (a) Temperature amplitude and (b) phase for a harmonically varying beam tip heating power, $P(t) = e^{i\omega t}$.

simulation and measurements is excellent for the reference device. This confirms that extraction of thermal parameters using the one-dimensional model is sound for this structure.

Second, a finite element model of the striped device was created and is shown in Fig 4. The temperature field was simulated at $\omega = 750\ s^{-1}$, which is the largest frequency used in the measurements. The temperature phase along a cut perpendicular to the heat flow is shown in Fig. 5. Here, uniformity is broken, and the phase varies considerably across the cantilever. The temperature in the regions of the cantilever where no metal is present lags behind that measured at the contacts. The one-dimensional model is therefore not applicable to this device. To minimize the observed effect, the design of the device must be modified.

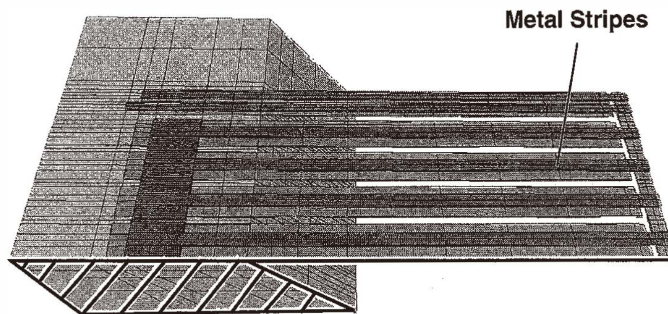

Fig. 4. Finite element model of the striped metal device. The dielectric layers have been removed to show the inner structure. Apart from the patterned metal layer, the mesh and boundary conditions correspond to those of Fig. 2.

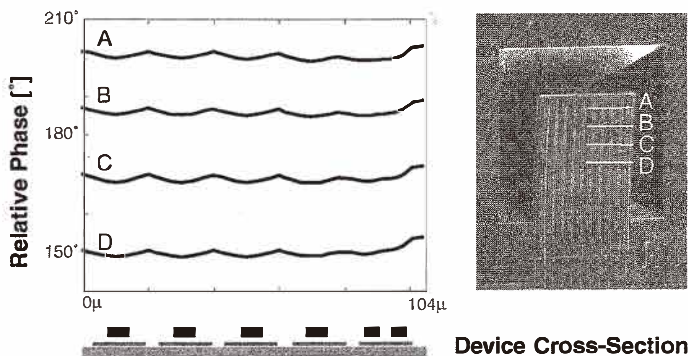

Fig. 5. Simulation results for the phase of the temperature for a fixed angular frequency of $750\ s^{-1}$. The nonuniformity in the phase across the device caused by the metal stripes is clearly visible.

The analysis method presented here is applicable to three further CMOS micromachined microsystems currently under development in our laboratory: an ultrasound resonator,[4] an electrical power converter[5] and an infrared detector.[6] A common feature of the first two systems is harmonic thermal excitation using an AC heating current. The latter system is heated using time-varying infrared radiation.

6. Conclusions

Harmonic modeling and simulation methods have been applied to characterize heat capacity measurement structures. The simulations were compared with measurements from an actual device and showed excellent agreement for one of the structures. Through simulation, it was shown that for the modified, nonuniform structure, 3-D effects must be considered and the design must be adjusted. The method described can be rapidly implemented in existing finite element software and is applicable to a wide range of thermally excited microsensors and actuators.

Acknowledgments

This work was supported by the Swiss Priority Program MINAST.

References

1 M. von Arx, O. Paul and H. Baltes: Thermoelectric Test Structures to Measure the Heat Capacity of CMOS Layer Sandwiches, Digest of Technical Papers of Transducers 97 (Chicago, June 1997).
2 M. von Arx, O. Paul and H. Baltes: Test Structure to Measure the Seebeck Coefficient of CMOS IC Polysilicon, IEEE Transactions on Semiconductor Manufacturing **10** (2) (1997) p. 201.
3 T. J. R. Hughes: The Finite Element Method (Prentice-Hall, Englewood Cliffs, 1987) Chap. 2.
4 O. Brand: Micromachined Resonators for Ultrasound Based Proximity Sensing, ETH Ph.D. Thesis No. 10896, (Physical Electronics Laboratory, Zurich 1996).
5 D. Jaeggi: Thermal Converters by CMOS Technology, ETH PhD Thesis No. 11567 (Physical Electronics Laboratory, Zurich, 1996).
6 N. Schneeberger, O. Paul and H. Baltes: Optimization of CMOS Infrared Detector Microsystems, SPIE Symposium on Micromachining and Microfabrication (Austin, Texas, October 14–16, 1996) p. 122.